Development of a USV Station-Keeping Controller

Edoardo I. Sarda, Ivan R. Bertaska, Ariel Qu and Karl D. von Ellenrieder,
Department of Ocean and Mechanical Engineering
Florida Atlantic University
Dania Beach, Florida
esarda@fau.edu

***Abstract*—The ability of unmanned surface vehicles (USVs) to maintain a fixed orientation and position for an extended period of time is essential for a variety of applications such as acoustic and optical localization and automated launch and recovery of other systems. The need for station-keeping capabilities on USVs requires collaboration between the controller and the propulsion system, both designed to allow the vehicle to perform this challenging maneuver. Small external perturbations, such as wind, waves and current, can have tremendous effects on low weight USVs. These can negatively affect the USV ability to hold its state, resulting in large errors or oscillations. A robust controller capable to account for unmodeled dynamics, which lead to significant deviations between simulated and experimental results, is therefore essential. After an appropriate propulsion system had been designed and installed on a USV, several station-keeping controllers were implemented and tested. Experimental testing of these controllers in environments of uncertain wind, current and wave disturbances show that the vehicle is best controlled by a nonlinear, backstepping, Multi-Input Multi-output (MIMO) PD controller. A Lagrangian multiplier method was used for control allocation. It is shown that a USV equipped with azimuthing electric propellers is capable to reach and maintain a specific configuration of heading and position for a period of ten or more minutes.**

Keywords— station-keeping, backstepping, nonlinear control unmanned surface vehicles, control allocation

I. INTRODUCTION & BACKGROUND

Autonomous Unmanned Surface Vehicles (USVs) can be utilized for a variety of tasks, thanks to their capability of acting independently with no need for human interaction. To be effective, a USV needs to be capable to autonomously perform a variety of distinct maneuvers, with navigation and station-keeping being essential in their roles. While the former is necessary to allow the vehicle to move within different locations, the latter allows on board systems to work in a controlled manner, minimizing possible sources of error. Among the most significant tasks that require a USV to station-keep are object localization and the launch and recovery of smaller subsystems. Underwater object localization via acoustics can require maintaining a fixed position and orientation for up to one minute. The performance of the acoustic sensors would be heavily affected if the vehicle drifts throughout this time. A similar case is that of optical localization using a camera. Here, image processing algorithms may require a few seconds; however, the performance is heavily affected if the vehicle drifts as small motions may result in dramatic changes in lighting conditions or image perspective. Launching and recovering an Autonomous Underwater Vehicle (AUV) from a USV is another complex task identified that requires precise collaboration between the USV on the surface and the AUV underwater. Generally, communication would be handled via underwater acoustics. The process can be simplified by fixing the USV position on the surface to reduce the number of moving objects, such that the problem is essentially transformed to the static docking of an AUV. Thus, enabling a USV to hold position and heading can transform complex tasks into simpler ones.

Nonlinear control of unmanned surface vehicles is currently an active area of research, with the majority of the effort devoted towards feedback linearization and backstepping methods [6], [15], [16], [17], [18], [19], [20], as well as sliding mode control [4], [16], [20]. However, the validation of USV control laws is often limited to numerical simulation or small-scale experiments, rather than full-scale sea trials [21]. In fact, even in more technologically mature areas such as AUV control, stabilization in the presence of environmental disturbances has only been partially addressed [22]. Several solutions have been proposed for the station-keeping of surface vehicles. In [23], experiments were performed on a small underactuated USV with high windage, where a feedforward wind model was modified to accommodate a PD-based heading autopilot. Switching between point and orientation stabilization and discontinuous control was employed to stabilize a marine vehicle to a point in the presence of a current using dipolar vector fields as guidance in [24] and [25]. Similarly, a hybrid approach was taken in [8] where multi-output PID controllers with and without acceleration feedback were used to stabilize a vehicle in high sea states by the use of an observer to estimate the peak wave frequency. The controller switched to controllers better suited to handle large disturbances as the peak wave frequency estimate decreased and, correspondingly, the sea state increased. Aguiar and Pascoal [22] devised a nonlinear adaptive controller capable of station-keeping an AUV with uncertain hydrodynamic parameters in the presence of an unknown current. Backstepping also was suggested in [9] as means to station-keep a fully-actuated vehicle, although environmental disturbances were not explicitly stated in the problem formulation.

This paper presents the formulation and experimental validation tests of three different station-keeping controllers for a 4.9 meter USV. A propulsion system was designed to enable the USV to maneuver in three degrees-of-freedom (DOF) – surge, sway and yaw. Several controllers were formulated to stabilize the system to desired position and heading. Although a trade-off always exists when trying to

simultaneously maintain heading and position, the optimal controller ought to minimize both position and heading error. An overview of the propulsion system design and experimental results from different alternatives of station-keeping control are presented.

II. THE USV

A. Overview

The USV used here is a Wave Adaptive Modular-Vehicle (WAM-V) USV16 (Fig. 1). It is a twin hull, pontoon style vessel designed and built by Marine Advanced Research, Inc. of Berkeley, CA USA.

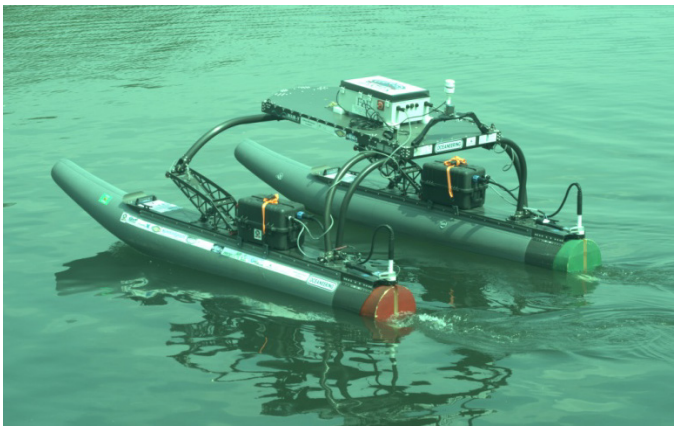

Fig. 1: The WAM-V USV16 during on-water station-keeping tests

The vessel structure consists of two inflatable pontoons, a payload tray connected to the pontoons by two supporting arches and a suspension system. The WAM-V is designed to mitigate the heave, pitch and roll response of the payload tray when the vehicle operates in surface waves. The vehicle's physical characteristics are shown in Table 1.

TABLE 1 - PRINCIPLE CHARACTERISTICS OF THE WAM-V USV16. THE LOCATION OF THE "KEEL" IS TAKEN AS THE BOTTOM OF THE PONTOONS. W.R.T. IS AN ACRONYM FOR THE PHRASE "WITH RESPECT TO".

Parameter	Value
Length Overall (L)	4.88 [m]
Length on the Waterline (LWL)	3.20 [m]
Draft (aft and mid-length)(lightship)	0.30 and 0.23 [m]
Beam Overall (B)	2.44 [m]
Beam on the Waterline (BWL)	2.39 [m]
Depth (keel to pontoon skid top)	0.43 [m]
Area of the Waterplane (AWP)	1.6 [m^2]
Centerline-to-centerline Side Hull Separation (BCC)	1.83 [m]
Length to Beam Ratio (L/B)	2.0
Volumetric Displacement (∇) (lightship)	0.5 [m^3]
Mass	180 [kg]
Longitudinal Center of Gravity (LCG) w.r.t. aft plane of engine pods	1.30 [m]

In addition to its standard characteristics, a custom designed propulsion system was implemented on the USV16 (Fig. 2). This includes two 120 N electric thrusters, each powered by a 12V lead acid battery, and two 160 N, 15 cm stroke, linear actuators capable of rotating the thrusters through an azimuthal angle of $\pm 45^o$ with respect to the vehicle's longitudinal direction (Fig. 3).

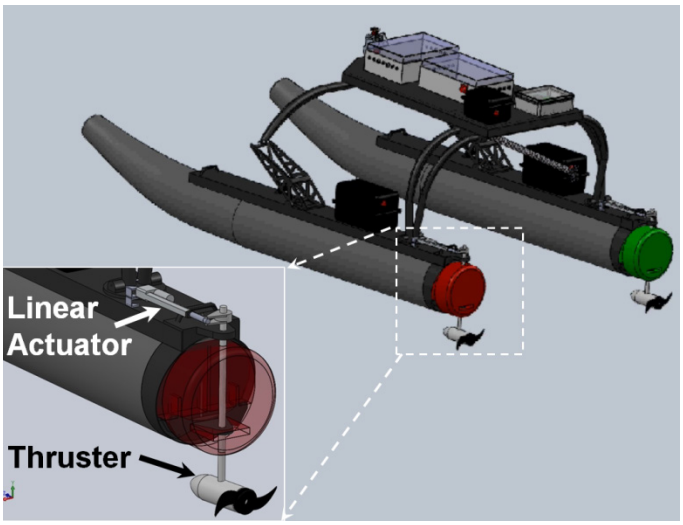

Fig. 2: WAM-V USV16 propulsion system CAD

Thrust on each pontoon (T_{port} and T_{stbd}) can therefore be directed in various directions based on the azimuth angle on each side (δ_{port} and δ_{stbd}), enabling the vehicle to output multiple combinations of forces and moments. The moment is calculated based on the moment arms (r_{port} and r_{stbd}), shown in Fig. 3. The configuration of the propulsion system permits the USV16 to move in surge, sway and yaw DOF so that it is a fully actuated system.

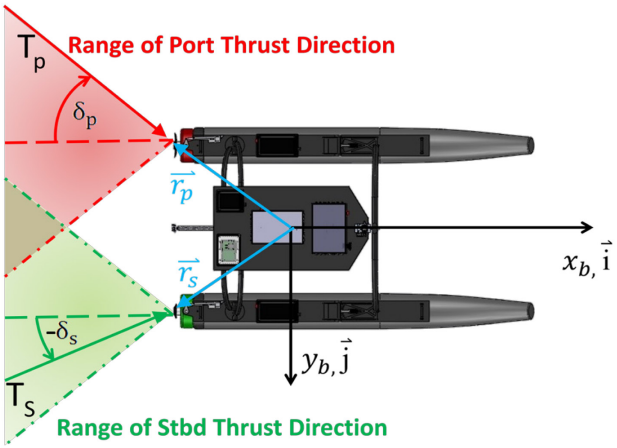

Fig. 3: Thrust Distribution on WAM-V USV16.

A guidance, navigation and control (GNC) system was implemented on the WAM-V USV16 to enable its autonomy [30]. The GNC system is housed in a plastic, water-proof box and contains a motherboard, single-board computer, inertial measurement unit (IMU) with global positioning system (GPS) capability, tilt-compensated digital compass, radio frequency

(RF) transceiver, and pulse width modulation (PWM) signal generator. A detailed summary of the GNC system can be found in [1]. For the purpose of this project, the key components of the GNC system are the sensor suite (IMU/GPS and digital compass), single-board computer, and RF transceiver. The IMU/GPS is an XSENS MTi-G sensor, which is used to estimate the position and orientation of the USV during operations. This information is relayed at 4Hz via the Lightweight Communication and Data Marshalling system [14] to the single board computer, where the low level control code is implemented. State data is also logged at 4Hz. The GPS is WAAS enabled and can provide up to 1 meter accuracy in both latitude and longitude, depending on cloud cover and satellite availability. The digital compass is used to monitor vehicle heading and has a resolution of 0.1 degrees. An RF receiver allows the user the option of maneuvering the USV under remote manual control or by autonomous navigation. A hand-held remote control is used for operating the thrusters and the actuators in manual mode and also for initiating autonomous operations.

B. *Equations of Motion*

The dynamic model of the WAM-V USV14 [2] was adapted to be utilized for the development of a station-keeping controller for the WAM-V USV16. This model was developed following the procedure described in [5], [29], [31]. The parameters in the model were changed to those of the USV16 in Table 1, but the hydrodynamics coefficient were kept the same. This was found to be acceptable since the two vehicles share a similar hull form and belong to the same family. More specifically, it can be stated that the WAM-V USV16 is a scaled up model of the WAM-V USV14. The development of this state space maneuvering model is described in [2]. Since these USVs are designed to operate on the water surface in low/medium sea states, the vehicle motion can be assumed to be planar with linear motion only in the x and y direction and rotation only about the z axis. Therefore, the USV16 motion is approximated using only three DOF: surge, sway and yaw. The following equations of motion were used to describe the USV16 dynamic model:

$$\boldsymbol{M}\dot{\boldsymbol{v}} + \boldsymbol{C}(\boldsymbol{v})\boldsymbol{v} + \boldsymbol{D}\boldsymbol{v} = \boldsymbol{\tau}\,, \tag{1}$$

$$\dot{\boldsymbol{\eta}} = \left[\dot{x}\ \dot{y}\ \dot{\psi}\right]^T\,, \tag{2}$$

$$\boldsymbol{v} = [u\ v\ r]^T\,. \tag{3}$$

Where $\boldsymbol{M}$ is the mass matrix, $\boldsymbol{C}(\boldsymbol{v})$ is the Coriolis matrix, $\boldsymbol{D}(\boldsymbol{v})$ is the drag matrix and $\boldsymbol{\tau}$ is the vector of the forces and moment generated by vehicle's thrusters. $\boldsymbol{M}$ and $\boldsymbol{C}(\boldsymbol{v})$ include both rigid body and added mass terms. The vector $\dot{\boldsymbol{\eta}}$ describes the vehicle's North $(\dot{x})$, East $(\dot{y})$ velocities and the angular velocity $(\dot{\psi})$ around the z axis in an inertial reference frame, $\boldsymbol{\eta} = [x, y, \psi]^T$, and the vector $\boldsymbol{v}$ contains the vehicle surge velocity (u), sway velocity (v) and yaw rate (r) in the body fixed frame. These two coordinate systems are illustrated in Fig. 4.

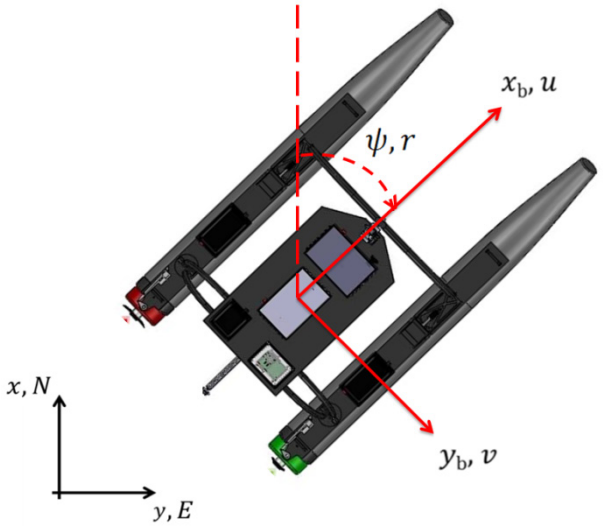

Fig. 4: Top view of WAM-V USV16 with body-fixed coordinate system overlaid. x_b and y_b denote vessel surge and sway axes, respectively.

The transformation matrix for converting from body-fixed to earth-fixed frames is given by the rotation matrix:

$$\boldsymbol{J}(\boldsymbol{\eta}) = \begin{bmatrix} \cos\psi & -\sin\psi & 0 \\ \sin\psi & \cos\psi & 0 \\ 0 & 0 & 1 \end{bmatrix}. \tag{4}$$

All the numerical values of the hydrodynamic coefficients used in the matrices presented in (1) are given in Table 2.

TABLE 2 - NUMERICAL VALUES OF WAM-V USV 16 HYDRODYNAMIC COEFFICIENTS

Parameters	Value
Mass Moment of Inertia about z axis	239.137 [kg*m^2]
Added Mass Coeff. in Surge Direction from Surge Acceleration ($X_{\dot{u}}$)	-3.7475 [kg]
Added Mass Coeff. in Sway Direction from Sway Acceleration ($Y_{\dot{v}}$)	-33.52 [kg]
Added Mass Coeff. in Sway Direction from Yaw Acceleration ($Y_{\dot{r}}$)	0 [kg*m]
Added Mass Coeff. from Yaw Accel. ($N_{\dot{r}}$)	-24.54 [kg*m^2]
Added Mass Coeff. from Sway Accel. ($N_{\dot{v}}$)	0 [kg*m]
Linear Drag Coeff. in Surge Direction(X_u)	-20 [kg/s]
Linear Drag Coeff. in Sway Direction (Y_v)	-150 [kg/s]
Linear Drag Coeff. in Sway Direction (Y_r)	0 [kg*m/s]
Linear Drag Moment Coeff. from Yaw Rate (N_r)	-0.3 [kg*m^2/s]
Linear Drag Moment Coeff. from Sway (N_v)	0 [kg*m/s]

The origin of the body-fixed axis is taken to be the center of gravity of the vehicle. After eliminating all the zero terms, the matrices used in the dynamic model of the vehicle (1) are as follows:

$$\boldsymbol{M} = \begin{bmatrix} m - X_{\dot{u}} & 0 & 0 \\ 0 & m - Y_{\dot{v}} & 0 \\ 0 & 0 & I_z - N_{\dot{r}} \end{bmatrix}, \tag{5}$$

$$\boldsymbol{C}(\boldsymbol{v}) = \begin{bmatrix} 0 & 0 & -(m - Y_{\dot{v}})v \\ 0 & 0 & (m - X_{\dot{u}})u \\ (m - Y_{\dot{v}})v & -(m - X_{\dot{u}})u & 0 \end{bmatrix}, \tag{6}$$

$$\boldsymbol{D} = -\begin{bmatrix} X_u & 0 & 0 \\ 0 & Y_v & 0 \\ 0 & 0 & N_r \end{bmatrix}, \tag{7}$$

$$\boldsymbol{\tau} = \begin{bmatrix} T_x \\ T_y \\ M_z \end{bmatrix}. \tag{8}$$

T_x and T_y denote the thrust generated in the x_b and y_b direction, respectively, and M_z is the resulting moment around the z_b axis. The forces caused by wind, waves and currents are not included in this model. Also, note that nonlinear drag was neglected in this model. This is considered acceptable since the velocities in both direction during station-keeping will approach zero very rapidly. More details about the derivation of the equations and the parameters used are presented in [2].

III. Station-Keeping Control

The lowest levels of motion control required for station-keeping are in position (x and y) and heading (ψ). Due to the configuration of the propulsion system, the USV16 can achieve its desired state in multiple ways. The methodology involved in selecting the optimal configuration for a desired state is highlighted in Section IV. Several controllers have been developed and implemented on the USV16 for the same purpose but with different formulations and characteristics. For all controllers, the output is the desired forces and torque on the vehicle $\boldsymbol{\tau}$ as in (8). Since the USV16 is propelled by twin motors located at the transom of each demihull, the output of the controller is then transformed in thrust and azimuth for port and starboard motor, $\{T_p, \alpha_p, T_s, \alpha_s\}$. This transformation is detailed in Section IV. The block diagram in Fig. 5 shows the control flow described. In this section, we derive the three controllers used for station-keeping on the USV16.

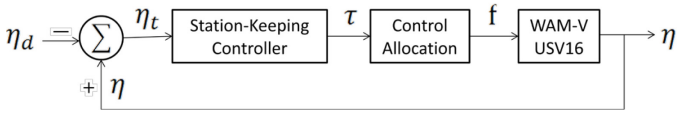

Fig. 5: Block Diagram of WAM-V USV 16 Control System

A. Proportional Derivative (PD) Control

A nonlinear Proportional Derivative (PD) controller similar to that in [8] was first derived to provide a baseline for the nonlinear controllers in the following sections. Let $\boldsymbol{\eta}_d$ be the desired pose of the vehicle in the earth-fixed frame, $\boldsymbol{\eta}_d = [x_d, y_d, \psi_d]^T$. An error vector is defined as the difference between the desired pose and the vehicle pose:

$$\boldsymbol{\eta}_t = \boldsymbol{\eta} - \boldsymbol{\eta}_d. \tag{9}$$

Owing to the orthogonality of (4), this error vector can be transformed into the body-fixed frame by $\boldsymbol{\eta}_t^b = \boldsymbol{J}(\boldsymbol{\eta})^T \boldsymbol{\eta}_t$. This leads to a nonlinear PD control law of the form

$$\boldsymbol{\tau} = -\boldsymbol{K}_P \boldsymbol{\eta}_t^b - \boldsymbol{K}_D \dot{\boldsymbol{\eta}}_t^b. \tag{10}$$

Where $\boldsymbol{K}_P$ and $\boldsymbol{K}_D$ are positive definite diagonal matrices. Gains for these matrices were first tuned in simulation for the vehicle and were then refined during field experiments.

B. Backstepping Control

Backstepping control theory was applied to station-keeping using the approach presented in [26] and [27]. Here only the final result with some necessary corrections are presented.

Since the performance of the PD controller, as implemented on the vehicle, was very different from that found during simulation, a MIMO backstepping controller was designed to overcome unmodeled dynamics and environmental disturbances. These two issues were considered to be the cause of high deviations between the simulated and experimental results. The implementation of a backstepping controller also circumvented possible difficulties often encountered when gain-scheduling techniques cannot be applied to linearized models. This is the case when trying to control surge and sway position (x, y) and yaw angle (ψ) simultaneously (station-keeping).

A reference trajectory is first defined as:

$$\dot{\boldsymbol{\eta}}_r = \dot{\boldsymbol{\eta}}_d - \boldsymbol{\Lambda}\boldsymbol{\eta}_t. \tag{11}$$

Here $\dot{\boldsymbol{\eta}}_d$ is the derivative of the desired state of the vehicle ($\dot{x}_\mathrm{d}$, $\dot{y}_\mathrm{d}$ and r_d), which in the case of set point station-keeping will all be zero, and $\boldsymbol{\Lambda}$ is a diagonal design matrix based on Lyapunov exponents. Two Lyapunov functions are considered in [27]. These allow the system to be feedback stabilizable, implying that a control law can be formulated to force the system to its desired state independently of its initial state. $\boldsymbol{\Lambda}$ represents the Lyapunov exponent gain vector. For station-keeping, $\boldsymbol{\Lambda}$ is designed based on various candidates frequencies. Since multiple candidates exist, the selection is

made by choosing the value that produces the slowest decay rate of the errors. Three different candidate were selected for $\boldsymbol{\Lambda}$:

$$\Lambda_1 = \frac{2}{3}\pi * f_r, \tag{12}$$

$$\Lambda_2 = f_s/5, \tag{13}$$

$$\Lambda_3 = \frac{1}{3} * t_u. \tag{14}$$

Where f_r is the lowest resonant frequency expected (0.5 Hz), f_s is the sampling frequency (4 Hz) and t_u is the largest unmodeled time delay (2 sec). Since (14) gives the minimum bandwidth, $\boldsymbol{\Lambda}$ takes the following numerical form:

$$\boldsymbol{\Lambda} = \begin{bmatrix} \Lambda_3 & 0 & 0 \\ 0 & \Lambda_3 & 0 \\ 0 & 0 & \Lambda_3 \end{bmatrix} = \begin{bmatrix} 0.16\,Hz & 0 & 0 \\ 0 & 0.16\,Hz & 0 \\ 0 & 0 & 0.16\,Hz \end{bmatrix}. \tag{15}$$

A measure of tracking also needs to be defined based on the Lyapunov exponents. This tracking surface is defined as:

$$\boldsymbol{s} = \dot{\boldsymbol{\eta}}_{\boldsymbol{t}} + \boldsymbol{\Lambda}\boldsymbol{\eta}_t. \tag{16}$$

The error feedback control law for station-keeping then has the following form:

$$\boldsymbol{\tau} = \boldsymbol{M}\boldsymbol{J}(\boldsymbol{\eta})^T\ddot{\boldsymbol{\eta}}_r + \boldsymbol{C}(\boldsymbol{v})\boldsymbol{J}(\boldsymbol{\eta})^T\dot{\boldsymbol{\eta}}_r + \boldsymbol{D}\boldsymbol{J}(\boldsymbol{\eta})^T\dot{\boldsymbol{\eta}}_r - \boldsymbol{J}(\boldsymbol{\eta})^T\boldsymbol{K}_d\boldsymbol{s} - \boldsymbol{J}(\boldsymbol{\eta})^T\boldsymbol{K}_p\boldsymbol{\eta}_t. \tag{17}$$

Where $\boldsymbol{J}(\boldsymbol{\eta})$, $\boldsymbol{M}$, $\boldsymbol{C}(\boldsymbol{v})$, $\boldsymbol{D}$ and $\boldsymbol{\tau}$ correspond to equations (4), (5), (6), (7), and (8) respectively, $\boldsymbol{K}_d$ and $\boldsymbol{K}_p$ are the derivative and proportional control gain matrices, respectively, $\dot{\boldsymbol{\eta}}_r$ and $\ddot{\boldsymbol{\eta}}_r$ are the derivatives of a defined virtual reference trajectory vector, $\boldsymbol{\eta}_t$ is the earth-fixed tracking error vector defined in (9), and $\boldsymbol{s}$ is the tracking surface based on a Lyapunov exponent described in [26].

The control gains are assigned in two diagonal matrices ($\boldsymbol{K}_d$ and $\boldsymbol{K}_p$) to eliminate errors in position, velocity, yaw and yaw rate. The gains were initially chosen by modeling the controller in simulation, then tuned based on the controller performance during in-water tests.

The block for the backstepping station-keeping controller described is provided in Fig. 6.

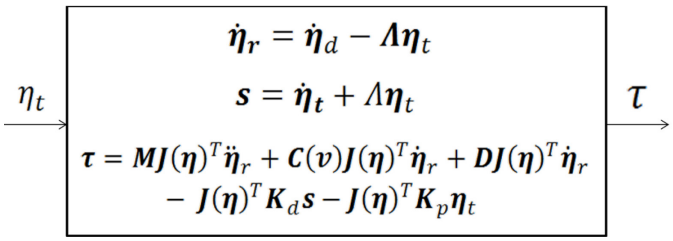

Fig. 6: Backstepping station-keeping controller

C. Sliding Mode Robust Control

Since the model used in the development of the backstepping controller was adapted from a different vehicle (WAM-V USV14), the necessity to develop a more robust form of control was evident. Robust control strategies, designed to yield good dynamic behaviors when confronted with modeling errors and unmodeled dynamics, were therefore introduced to develop a sliding mode station-keeping controller. In general, for all control systems, a trade-off between robustness and performance can be identified, therefore the choice of optimal controller is not always trivial and may depend on specific configurations and external factors [27].

Sliding mode control is a well-known approach to robust control by nonlinear feedback. A sliding surface function is first defined, similarly to (16), as:

$$\boldsymbol{s} = \dot{\boldsymbol{\eta}}_t + 2\boldsymbol{\Lambda}\boldsymbol{\eta}_t + \boldsymbol{\Lambda}^2\int_0^t \boldsymbol{\eta}_t dt. \tag{18}$$

A reference trajectory is also defined, similarly as in (11):

$$\dot{\boldsymbol{\eta}}_r = \dot{\boldsymbol{\eta}}_d - 2\boldsymbol{\Lambda}\boldsymbol{\eta}_t - \boldsymbol{\Lambda}^2\int_0^t \boldsymbol{\eta}_t dt. \tag{19}$$

Where all the terms are defined as in (11), (15) and (16). The control law then ensures that if the system deviates from this surface, it is forced back to it. Once on the surface, the under-modeled system reduces to an exponentially stable, second-order system. The system's response therefore depends heavily on the choice of the sliding surface. As a result the system will possess considerable robustness against external perturbations and incorrectly modeled dynamics. However, as it's shown in the experimental results, the system proves to be quite sensitive to these disturbances in the initial transition phase.

The sliding mode control law is similar to (17) and is defined as follows:

$$\boldsymbol{\tau} = \boldsymbol{M}\boldsymbol{J}(\boldsymbol{\eta})^T\ddot{\boldsymbol{\eta}}_r + \boldsymbol{C}(\boldsymbol{v})\boldsymbol{J}(\boldsymbol{\eta})^T\dot{\boldsymbol{\eta}}_r + \boldsymbol{D}(\boldsymbol{v})\boldsymbol{J}(\boldsymbol{\eta})^T\dot{\boldsymbol{\eta}}_r - \boldsymbol{J}(\boldsymbol{\eta})^T\boldsymbol{R} * sat(\boldsymbol{E}^{-1} * \boldsymbol{s}). \tag{20}$$

It can be noted that (20) is the same as (17) except for the last term, which includes the bound on the uncertainties $\boldsymbol{R}$ and the boundary layer thickness $\boldsymbol{E}$ around the sliding surface **s**, in place of $\boldsymbol{K}_d$ and $\boldsymbol{K}_p$. The saturation function is used instead of

the traditional signum function to reduce the chattering effect [27].

The saturation function is the main factor that differentiates the sliding mode controller. In (20), the bound on the uncertainties $\boldsymbol{R}$ acts similarly to controller gains $\boldsymbol{K}_d$ and $\boldsymbol{K}_p$in (17). The difference is that, once the system enters the boundary layer $\boldsymbol{E}^{-1}\boldsymbol{s}$, a discontinuous control signal is applied, forcing the system to slide along a cross-section of the system normal behavior. The illustration of this signal for each element in $\boldsymbol{R}$ and $\boldsymbol{E}$ is given in Fig. 7.

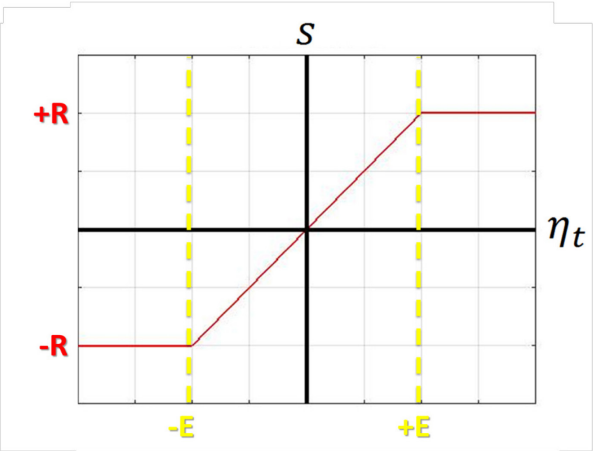

Fig. 7: Illustration of Saturation Function for a single saturation argument for Sliding Mode Controller

Both, the bound on the uncertainties matrix $\boldsymbol{R}$ and the boundary layer thickness $\boldsymbol{E}$, were initially selected based on the results obtained testing the PD and the backstepping controllers previously described, then tuned during in-water testing.

The control block for the sliding mode station-keeping controller described is provided in Fig. 8

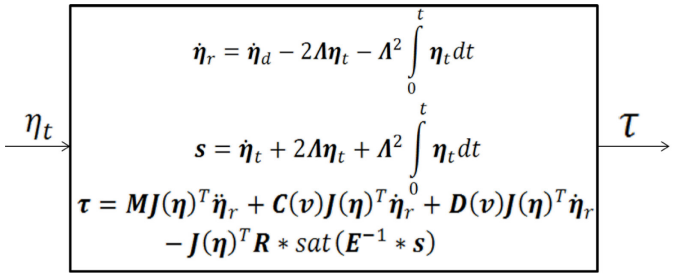

Fig. 8: Sliding Mode station-keeping controller

IV. Control Allocation

Azimuthing thruster configurations such as those found on the USV16 create an overactuated system, since multiple solutions to the controller output $\boldsymbol{\tau}$ can be found in terms of propeller thrust and azimuth angle (Fig. 3). This is formulated as an optimization problem, and techniques such as linear programming [9], [10], quadratic programming [11], and evolutionary algorithms [12] can be used to find an optimal solution. Actuator dynamics create constraints on this system, leading to a constrained nonlinear optimization problem, which is nontrivial to solve. An alternative to this method is to use a Lagrangian multiplier approach as described in [9]. A summary of our approach is presented below.

A. Extended Force Representation

For the m outputs of the controller, $\boldsymbol{\tau} \in \mathbb{R}^m$, let $\mathbf{f} \in \mathbb{R}^{2r}$ be the actuator forces in the surge and sway directions at each of the r actuators,

$$\mathbf{f} = \left[F_{x_1}\, F_{y_1} \ldots F_{x_i}\, F_{y_i} \ldots F_{x_r}\, F_{y_r}\right]^T. \tag{21}$$

A transformation matrix $\boldsymbol{T} \in \mathbb{R}^{2r\times m}$ from the controller output force $\boldsymbol{\tau}$ to the actuator frame force vector $\mathbf{f}$ can be defined as

$$\boldsymbol{\tau} = \boldsymbol{T}\mathbf{f}. \tag{22}$$

An extended thrust representation, as described in [13], is used to define $\boldsymbol{T}$,

$$\boldsymbol{\tau} = \begin{bmatrix} 1 & 0 & \ldots & 1 & 0 \\ 0 & 1 & \ldots & 0 & 1 \\ -l_{y_1} & l_{x_1} & \ldots & -l_{y_r} & l_{x_r} \end{bmatrix} \begin{bmatrix} F_{x_1} \\ F_{y_1} \\ \vdots \\ F_{x_r} \\ F_{y_r} \end{bmatrix}, \tag{23}$$

The constants l_{x_i} and l_{y_i} represent the longitudinal and lateral distances to the ith actuator measured with respect to the vehicle center of gravity. The solution to the allocation problem now rests in finding an inverse to the rectangular transformation matrix $\boldsymbol{T}$.

B. Lagrangian Multiplier Solution

A cost function C is set up to minimize the force output from each actuator subject to a positive definite weight matrix $\mathbf{W} \in \mathbb{R}^{2r\times 2r}$,

$$\min_{\mathbf{f}}\{C = \mathbf{f}^{\mathrm{T}}\mathbf{W}\mathbf{f}\}, \tag{24}$$

The optimization problem in (24) is subject to the constraint $\boldsymbol{\tau} - \mathbf{T}\mathbf{f} = \mathbf{0}$, i.e., the error between the desired control forces and the attainable control forces is minimized. The weight matrix $\mathbf{W}$ is set to skew the control forces towards the most efficient actuators. This is especially important for systems with rudders or control fins, as these actuators provide greater control authority with less power consumption.

A Lagrangian is then set up as in [3],

$$L(\mathbf{f}, \boldsymbol{\lambda}) = \mathbf{f}^{\mathrm{T}}\mathbf{W}\mathbf{f} + \boldsymbol{\lambda}^{\mathrm{T}}(\boldsymbol{\tau} - \mathbf{T}\mathbf{f}). \tag{25}$$

Differentiating (25) with respect to **f,** one can show that the solution for $\mathbf{f}$ reduces to $\mathbf{f} = \mathbf{T}_{\mathbf{w}}^{\dagger}\boldsymbol{\tau}$, where the inverse of the weighted transformation matrix is,

$$\mathbf{T}_{\mathbf{w}}^{\dagger} = \mathbf{W}^{-1}\mathbf{T}^{\mathrm{T}}(\mathbf{T}\mathbf{W}^{-1}\mathbf{T}^{\mathrm{T}})^{-1}. \quad (26)$$

If a vehicle has port/starboard symmetry with identical actuators, the weight matrix $\mathbf{W}$ can be taken as the identity matrix, $\mathbf{W} = \mathbf{I} \in \mathbb{R}^{2r\times 2r}$, and the inverse of the transformation matrix becomes the Moore-Penrose pseudoinverse of the transformation matrix, $\mathbf{T}_{\mathbf{w}}^{\dagger} = \mathbf{T}^{\mathrm{T}}(\mathbf{T}\mathbf{T}^{\mathrm{T}})^{-1}$.

Once the component force vector $\mathbf{f}$ is found, it is trivial to apply a four-quadrant *arctan* function to find the rotation angle and calculate the magnitude of the thrust at each propeller. Due to the fact that thrust characteristics aren't precisely modeled within the allocation scheme, the resultant force and angle at each propeller is low-pass filtered with a user-set time constant to maintain a feasible rotation rate in practice. The low-pass filters used here are simple first order, infinite impulse response filters with a single time constant to determine the cross-over frequency of each's response. This is set to conservatively match the actuator dynamics. Two separate low-pass filters were used to filter the control allocation output for the azimuth as well as thrust of each motor. In effect, the time constant for the thrust filter was an order of magnitude greater than that of the azimuth filter.

Each propeller is capable of achieving a rotation from -45° to 45° – implying that a 180° offset from those values are also attainable by reversing the propeller. A logic scheme is implemented on top of the allocation that stops the thrust if the allocation requests an unachievable angle, and reverses it if an angle from -135° to 135° is given. Careful tuning of controller parameters are necessary to ensure that these constraints are not violated. This approach produces a computationally efficient answer to the overallocation optimization problem, capable of being implemented on an embedded system within the vehicle.

V. Station-Keeping Experiments

A series of experiments were performed in the calm water sections of the Intracoastal Waterway in Dania Beach, FL, USA to test the performance of the station-keeping controllers described in Section III and the control allocation scheme in Section IV. In order for the vehicle to operate effectively, it cannot be used in sea states greater than 1, wind speeds greater than 15 knots, wave heights greater than 0.2 meters and environments with heavy currents. To minimize the effect of waves on the vehicle, no tests were performed in the open ocean. To estimate the wind disturbance, a wind sensor [28] was added to the system, but its measurement was not accounted for by any of the controllers used. At this stage, the vehicle lacked an appropriate sensor to measure the water current. However the effect of the current could be estimated by letting the vehicle drift for period of time and recording its position. The change in position during the drift can then be assumed to depend solely on wind and current. Assuming the motion caused by the wind can be estimated using the sensor [28], then the rest of the motion must be caused by current.

A small map illustrating the locations where the experiments were conducted is shown in Fig. 9. The vehicle was free to drift over a 5 minute time span is also shown in Fig. 9. Two different locations were chosen to perform the experiments; each controller described in Section III was then tested at each location. The locations were selected to expose the vehicle to maximum (Location 1) and minimum (Location 2) local environmental disturbances. The desired heading of the vehicle was also chosen to reproduce the harshest (Location 1) and the most friendly (Location 1) scenarios. Since the propulsion system mounted on the WAM-V does not allow pure sway motion, the most difficult configuration to achieve will be one that requires such maneuver. At location 1 the vehicle's desired heading is 90 degrees off the disturbance direction - therefore, the controller will output a high force in the sway direction to counteract the disturbance, recreating the harshest scenario. The WAM-V is designed to navigate primarily in the surge direction - therefore this type of motion is considered the simplest to achieve. At Location 2, the vehicle's desired heading is in the opposite direction of the disturbance, therefore the controller will output a high force in the surge direction. This maneuver can be easily achieved and therefore this is considered a friendly scenario.

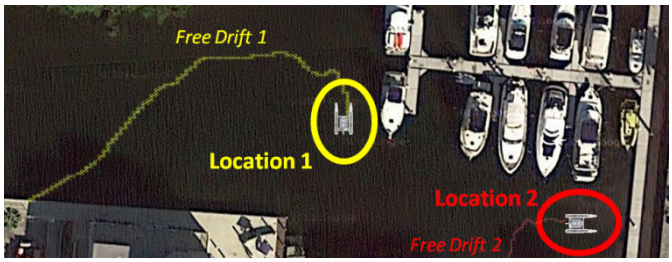

Fig. 9: Testing Locations and Drifting Conditions

The wind speed at Location 1 was collected during the free drift of the vehicle and it is shown in Fig. 10. The wind direction on average was due south.

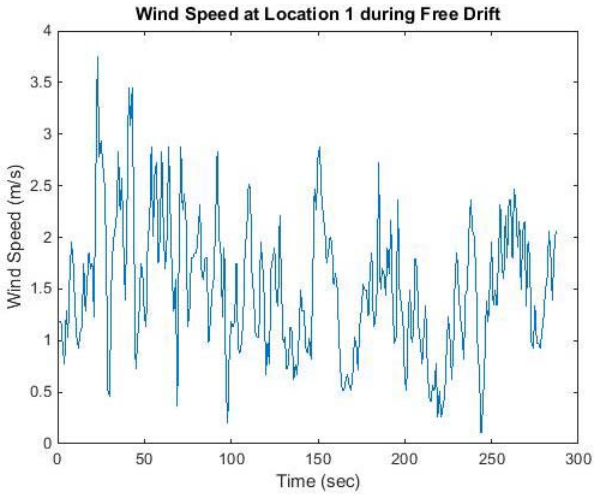

Fig. 10: Wind Speed and Direction during experiments

To start the experiments, the vehicle was first set to its desired state (shown in Fig. 9) using the remote controller, then engaged into autonomous mode and commanded to maintain the current state. Heading and position error were then recorded. The results for the PD station-keeping controller operating at location 1 are shown in Fig. 11.

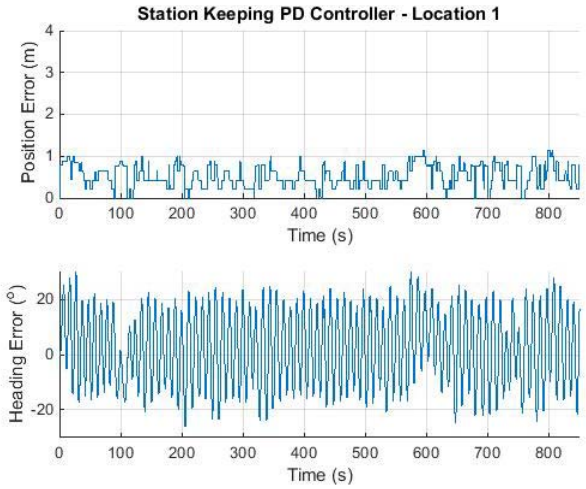

Fig. 11: Results for PD Station-Keeping controller operating at Location 1

In order to maintain position, the PD controller outputs heavily fluctuates, causing the vehicle to rotate. This translates in large and steady oscillation of the vehicle's heading throughout the entire experiment. Gain tuning techniques on the PD controller are not sufficient to reduce the heading error, since minimal improvements in the heading performance cause drastic increase of position error. The results for the backstepping station-keeping controller performing at location 1 (Fig. 12) show a major improvement in heading error, as compared to the PD controller.

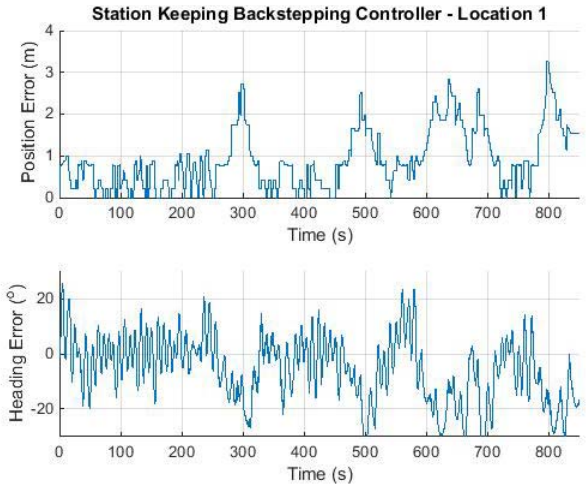

Fig. 12: Results for Backstepping Station-Keeping Controller operating at Location 1

The backstepping controller is capable of maintaining a small position error, while also minimizing the heading error. Although the amplitude of vehicle's heading oscillation was reduced, it is still evident that the heading error changes from positive to negative values over short periods of time (less than 30 seconds), resulting in jerky movements of the vehicle. This can be a major issue for certain applications. An improvement is observable in Fig. 13, where the results for the sliding mode station-keeping controller also operating at Location 1 can be seen.

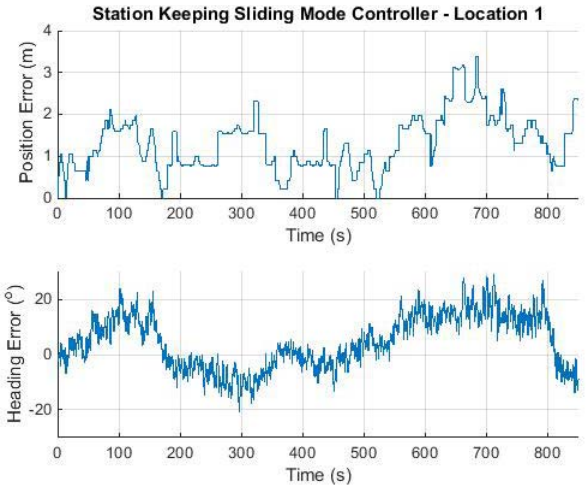

Fig. 13: Results for Sliding Mode Station-Keeping Controller operating at Location 1

The sliding mode controller is able to outperform the PD and the backstepping controllers in heading performance, without a significant increase in position error. The results for the sliding mode controller show that oscillations in heading error can be identified at two very distinct frequencies. The first frequency corresponds to very small variations (less than 5 degrees) that are usually irrelevant for any application. The second one takes place over much longer periods of time (~600 seconds) and therefore happens very slowly. Due to the nature of marine vehicles and the environment in which they operate, it is almost impossible to eliminate these oscillations completely. However, their frequency and amplitude can be minimized based on the application.

The performance of all the controllers at Location 2 is shown in Fig. 14, Fig. 15, and Fig. 16. As expected, all controllers performed slightly better than at Location 1, since the desired state of the vehicle was simpler to achieve. Overall the results at Location 2 are coherent with the data obtained at Location 1. The PD controller still creates highly fluctuating heading error that allows the vehicle to maintain the position error minimum. The backstepping controller brings improvement by reducing the oscillation in heading, while the position error is kept unchanged. With the sliding mode controller, the oscillation in heading is almost invisible until the data is plotted, however this results in a higher position error. These results proved that the sliding mode controller creates a more robust system, with less errors oscillations, at the cost of a decrease in positioning performance.

The experimental results differ from those in simulation. This suggests that unmodeled environmental disturbances play a major role in affecting the performance of the controllers and therefore should be included in the model. Also, the

improvement in performance at Location 2 proves that the vehicle's propulsion system has major limitations that the controller alone cannot overcome, therefore resulting in bigger errors.

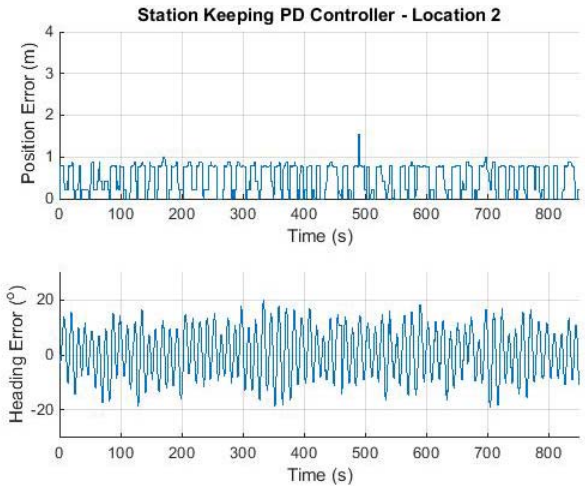

Fig. 14: Errors for PD Station-keeping Controller at Location 2

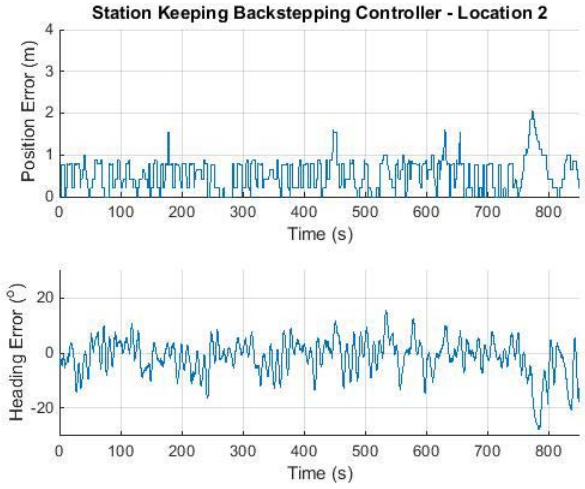

Fig. 15: Results for Backstepping Station-keeping Controller at Location 2

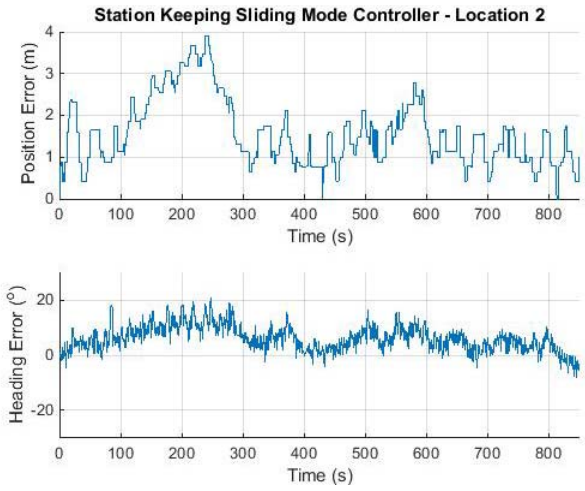

Fig. 16: Results for Sliding Mode Station-keeping Controller at Location 2

The mean (μ) and Standard Deviation (σ) of heading and position error for each controller at both location is given in Table 3.

TABLE 3
MEAN AND STANDARD DEVIATION OF EACH CONTROLLER FOR LOCATION 1 AND LOCATION 2

Controller:	Sliding Mode	Backstepping	PD
Position Error (m) at Location 1:	μ = 1.49 σ = 0.91	μ = 0.99 σ = 0.72	μ = 0.53 σ = 0.26
Heading Error (deg) at Location 1:	μ = 9.18 σ = 6.03	μ = 10.54 σ = 8.33	μ = 11.90 σ = 6.71
Position Error (m) at Location 2:	μ = 1.51 σ = 0.8	μ = 0.55 σ = 0.39	μ = 0.50 σ = 0.35
Heading Error (deg) at Location 2:	μ = 6.05 σ = 4.04	μ = 4.76 σ = 4.25	μ = 8.39 σ = 6.06

All experiments described were repeated ten times starting with non-zero errors in both position and heading. Except for an initial time of less than one minute, necessary for the system to reach steady state, the results were extremely similar the ones shown in Fig. 11, Fig. 12, Fig. 13, Fig. 14, Fig. 15 and Fig. 16.

VI. CONCLUSIONS

Three distinct station-keeping controllers for a USV were described in this paper. The results have shown that all three controllers performed sufficiently well, thanks to a custom designed propulsion system that allowed the vehicle to be fully actuated. Overall, the sliding mode station-keeping controller was shown to be the most robust and the backstepping controller was the most precise. This leads to the conclusion that different station-keeping controllers may be utilized depending on the application. Localization of objects that are placed a significant distance away from the vehicle may require the USV heading to be very stable, giving the camera time to adapt, while small and slow variations of the USV position may not affect image processing algorithms as much. The sliding mode controller developed provides the best fit for this scenario. In contrast, precise acoustic localization requires the need to maintain a specific position for extended periods of time (more than one minute). In this case the backstepping controller described would be the best fit.

All controllers were highly affected by environmental disturbances, especially wind and current. Future studies may include the possibility of adding sensors to system to the measure these disturbances. These measurements can then be fed back to each controller allowing them to formulate a more precise response. Another field of study may include a redesign of the propulsion system to supply the vehicle more thrust in all directions.

ACKNOWLEDGMENT

This work is partially supported by the U.S. Office of Naval Research under Grant N000141410274, Program Manager K. Cooper. I.R. Bertaska gratefully acknowledges the support of the Link Foundation Ocean Engineering and Instrumentation Ph.D. Fellowship Program. The authors would also like to

thank the FAU/VU RobotX team for their assistance with hardware development.

REFERENCES

[1] Marquardt, J. G. Alvarez, J. and von Ellenrieder, K. D. (2014) Characterization and System Identification of an Unmanned Amphibious Tracked Vehicle. *IEEE J Oceanic Engng. In Press.*

[2] Marquardt, J. G. Alvarez, J. and von Ellenrieder, K. D. (2014) Characterization and System Identification of an Unmanned Amphibious Tracked Vehicle. *IEEE J. Oceanic Engineering*. **39**(4):641-661.

[3] T. I. Fossen, *Guidance and Control of Ocean Vehicles*. Chichester: John Wiley and Sons Ltd, 1994.

[4] Alvarez, J., Bertaska, I., and von Ellenrieder, K. 2013. "Nonlinear Adaptive Control of an Amphibious Vehicle." In Proc. ASME *Dynamic Systems Control Conference,* 2013.

[5] Bertaska, I. R., Alvarez, J., et.al., "Experimental Evaluation of Approach Behavior for Autonomous Surface Vehicles." In Proc. ASME *Dynamic Systems Control Conference,* 2013.

[6] Liao, Yulei; Pang, Yongjie; Wan, Lei., "Combined speed and yaw control of underactuated unmanned surface vehicles," *2010 2nd International Asia Conference on Informatics in Control, Automation and Robotics (CAR),* vol.1, pp. 157-161, March 2010.

[7] Slotine, Jean-Jaques E.; Li, Weiping, *Applied Nonlinear Control.* New Jersey: Prentice Hall, 1991.

[8] Nguyen, T.D., Sorenson, A.J., Quek, S.T. "Design of hybrid controller for dynamic positioning from calm to extreme sea conditions," *Automatica 43(5)*, pp 768-785, 2007.

[9] Fossen, Thor I., and Tor A. Johansen. "A survey of control allocation methods for ships and underwater vehicles." *Control and Automation, 2006. MED'06. 14th Mediterranean Conference on*. IEEE, 2006.

[10] Webster, William C., and Joao Sousa. "Optimum allocation for multiple thrusters." *Proc. of the Int. Society of Offshore and Polar Engineers Conference (ISOPE'99)*. 1999.

[11] Johansen, Tor Arne, Thor I. Fossen, and Stig P. Berge. "Constrained nonlinear control allocation with singularity avoidance using sequential quadratic programming." *Control Systems Technology, IEEE Transactions on* 12.1 (2004): 211-216.

[12] Yadav, Parikshit, et al. "Optimal Thrust Allocation for Semisubmersible Oil Rig Platforms Using Improved Harmony Search Algorithm." *Oceanic Engineering, IEEE Journal of* 39.3 (2014): 526-539.

[13] Sørdalen, O. J. "Optimal thrust allocation for marine vessels." Control Engineering Practice 5.9 (1997): 1223-1231.

[14] Huang, Albert S., Edwin Olson, and David C. Moore. "LCM: Lightweight communications and marshalling." *Intelligent robots and systems (IROS), 2010 IEEE/RSJ international conference on*. IEEE, 2010.

[15] Fossen, Thor I., and Jan P. Strand. "Tutorial on nonlinear backstepping: applications to ship control." *Modeling, identification and control* 20.2 (1999): 83-134.

[16] Ashrafiuon, Hashem, et al. "Sliding-mode tracking control of surface vessels." *Industrial Electronics, IEEE Transactions on* 55.11 (2008): 4004-4012.

[17] Sonnenburg, Christian R., and Craig A. Woolsey. "Modeling, identification, and control of an unmanned surface vehicle." *Journal of Field Robotics* 30.3 (2013): 371-398.

[18] Aguiar, Antonio Pedro, and Joao Pedro Hespanha. "Position tracking of underactuated vehicles." *American Control Conference, 2003. Proceedings of the 2003*. Vol. 3. IEEE, 2003.

[19] Do, K. D. "Practical control of underactuated ships." *Ocean Engineering* 37.13 (2010): 1111-1119.

[20] Mahini, Farshad, and Hashem Ashrafiuon. "Autonomous Surface Vessel Target Tracking Experiments in Simulated Rough Sea Conditions." *ASME 2012 5th Annual Dynamic Systems and Control Conference joint with the JSME 2012 11th Motion and Vibration Conference*. American Society of Mechanical Engineers, 2012.

[21] Ashrafiuon, Hashem, Kenneth R. Muske, and Lucas C. McNinch. "Review of nonlinear tracking and setpoint control approaches for autonomous underactuated marine vehicles." American Control Conference (ACC), 2010. IEEE, 2010.

[22] Aguiar, A. Pedro, and António M. Pascoal. "Dynamic positioning and way-point tracking of underactuated AUVs in the presence of ocean currents." *International Journal of Control* 80.7 (2007): 1092-1108.

[23] Pereira, Arvind, Jnaneshwar Das, and G. Sukhatme. "An experimental study of station keeping on an underactuated ASV." *Intelligent Robots and Systems, 2008. IROS 2008. IEEE/RSJ International Conference on*. IEEE, 2008.

[24] Panagou, Dimitra, and Kostas J. Kyriakopoulos. "Switching control approach for the robust practical stabilization of a unicycle-like marine vehicle under non-vanishing perturbations." *Robotics and Automation (ICRA), 2011 IEEE International Conference on*. IEEE, 2011.

[25] Panagou, Dimitra, and Kostas J. Kyriakopoulos. "Dynamic positioning for an underactuated marine vehicle using hybrid control." International Journal of Control 87.2 (2014): 264-280.

[26] H.g. Sage, M. F. De Mathelin and E. Ostertag, "Rboust Control of robot manipulators: a survey,", Int. J. Control, 1999

[27] T.I. Fossen and J. P. Strand, "Tutorial on nonlinear Backstepping: Application to Ship Contro," Modeling, Identification and Control, 1999

[28] Qu, H. Sarda, E. I. Bertaska, I. R. & von Ellenrieder, K. D. (2015) "Wind Feed-forward Control of a USV," *In MTS/IEEE Oceans-Genova, 2015 – Genova, May 2015* (pp. 1-10).

[29] Mišković, N., Vukić, Z., Bibuli, M., Bruzzone, G., & Caccia, M. (2011). "Fast in-field identification of unmanned marine vehicles." *Journal of Field Robotics*,*28*(1), 101-120.

[30] Caccia, M., Bibuli, M., Bono, R., & Bruzzone, G. (2008). "Basic Navigation, Guidance and Control on an Unmanned Surface Vehicle," *Journal of Autonomous Robots*, *5*(4), 349-365.

[31] Caccia, M., Bruzzone, G, & Bono, R.. (2008). "A practical approach to modeling and identification of a small autonomous surface craft" IEEE *Journal of Oceanic Engineering*, *32*(2), 133-145.